A Proposal for an X-Ray Free-Electron Laser Oscillator with an Energy-Recovery Linac

Kwang-Je Kim,[1] Yuri Shvyd'ko,[1] and Sven Reiche[2]

[1]*Advanced Photon Source, Argonne National Laboratory, Argonne, Illinois 60439, USA*
[2]*UCLA, Physics and Astronomy Department, Los Angeles, California 90095, USA*

(Received 14 March 2008; published 17 June 2008)

We show that a free-electron laser oscillator generating x rays with wavelengths of about 1 Å is feasible using ultralow emittance electron beams of a multi-GeV energy-recovery linac, combined with a low-loss crystal cavity. The device will produce x-ray pulses with 10^9 photons at a repetition rate of 1–100 MHz. The pulses are temporarily and transversely coherent, with a rms bandwidth of about 2 meV, and rms pulse length of about 1 ps.

DOI: 10.1103/PhysRevLett.100.244802 PACS numbers: 41.60.Cr, 41.50.+h, 42.55.Vc

In this Letter, we propose a fully coherent source of x rays with the peak brightness comparable to that of the self-amplified spontaneous emission (SASE) from high-gain free-electron lasers (FELs) [1–3]. The average brightness is predicted to be higher by several orders of magnitudes. The key components are a continuous sequence of ultralow emittance electron bunches from a multi-GeV energy-recovery linac (ERL) [4–6] and a low-loss optical cavity constructed from high-reflectivity crystals. The electron bunches from an ERL are not suitable for *high-gain* FELs due to its relatively small charge density. However, as we show here, an x-ray FEL is feasible in an *oscillator* configuration taking advantage of repeated low-gain amplifications. Such a device will be referred to as an x-ray FEL oscillator (X-FELO). X-FELOs can significantly enhance the capabilities of the future ERL-based x-ray facilities.

Use of crystals for X-FELO was first proposed in 1984 [7] when accelerators producing electron beams of suitable qualities were not known yet. More recently, the x-ray cavity to improve the coherence of high-gain x-ray FELs was considered in [8] and studied in detail in [9]. The coherence of high-gain FEL can also be improved by a self-seeding scheme without involving an x-ray cavity [10].

The principles of an FEL oscillator are well known [11]. A light pulse trapped in an optical cavity and an electron bunch from an accelerator meet at the entrance of an undulator and travel together. The amplified light pulse at the end of the undulator is reflected back to the entrance where it meets a fresh electron bunch, and so on. The pulse evolves from initially incoherent spontaneous emission to a coherent pulse as its intensity rises exponentially, if $(1 + g)r > 1$, where g is the gain (relative increase in the optical intensity per pass), and r is the round-trip reflectivity in the cavity. The gain decreases at high intensity due to overmodulation and the system reaches a steady state, i.e., *saturates*, when $(1 + g)r = 1$.

The high-reflectivity at normal-incidence required for an X-FELO cavity can be obtained by using crystals composed of low-Z atoms with high Debye temperature, such as C (diamond), BeO, SiC, or $\alpha - Al_2O_3$ (sapphire), etc. [12]. As an example, Fig. 1 shows the reflectivity and transmissivity of sapphire crystals as a function of the photon energy at normal incidence to the (0 0 0 30) atomic planes for two different crystal thicknesses d. The crystal with $d = 0.20$ mm is thick enough to ensure the highest reflectivity of $R = 0.96$ and thin enough to minimize the heat load due to x-ray absorption. The $d = 0.07$ mm crystal will allow $T \simeq 4\%$ transmission for out coupling of the X-FELO radiation. The crystals are assumed to be at 30 K. This ensures a high peak reflectivity, a low sensitivity of the interplanar spacing to crystal temperature, and a very high thermal conductivity. There is a valid concern about the availability of high-quality crystals. However, since the X-FELO beam size on the crystals will be small, about 0.2 mm in diameter, *small* high-quality single crystals seem to be feasible through selection from bulk crystals. High, almost theoretical, reflectivity in backscattering from the (0 0 0 30) atomic planes was demonstrated in the experi-

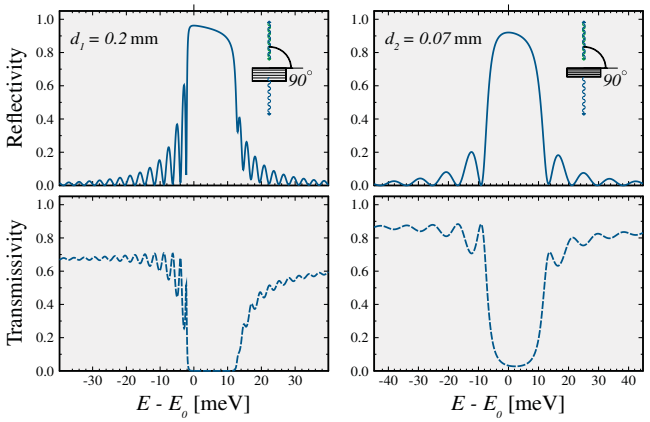

FIG. 1 (color). Reflectivity and transmissivity of x rays at normal incidence to the (0 0 0 30) atomic planes in $\alpha - Al_2O_3$. Crystal temperature $T = 30$ K, $E_0 = 14.326$ keV. The calculations have been performed using dynamical diffraction theory with the crystal data as in [12].

ment on the first x-ray Fabry-Pérot interferometer [13]. An even higher reflectivity, $R \simeq 0.99$, is predicted for diamond crystals. However, diamond crystals should be used in an off-normal-incidence configuration to avoid losses due to the multiple beam diffraction (see [12] for more details and references).

An optical cavity for X-FELO must also provide focusing to control the intracavity mode profile. Bending the crystals is not desirable since even a very gentle bending with a curvature radius of 50 m can significantly reduce the reflectivity. A promising option is to use parabolic compound refractive lenses (CRL) [14]. Two Be parabolic CRLs, each with a radius of 0.33 mm, have a focal distance of 50 m and a very high transmissivity of $T = 0.997$, assuming surface microroughness less than 0.3 μm and a beam size of 0.2 mm. A grazing-incidence ellipsoidal mirror can be used to focus and also to close the loop when the Bragg mirrors are not in the exact backscattering configuration.

Three schemes for x-ray cavities are shown in Fig. 2. Scheme (a) is a two-bounce system using the two normal-incidence sapphire crystals with reflectivities as in Fig. 1, and the CRLs. Scheme (b) uses two diamond crystals with the (444) Bragg reflection slightly off from the exact backscattering for 12.04-keV x rays. A grazing-incidence ellipsoidal mirror focuses the beam and closes the loop. Scheme (c) is designed specially for $E = 14.4125$ keV photons for nuclear resonance scattering experiments with ^{57}Fe [15]. It uses two sapphire crystals at an angle of incidence of 6.287°, the (201) reflection from a SiO_2 crystal closes the loop, and CRLs are used for focusing. Taking into account all losses from crystals and focusing

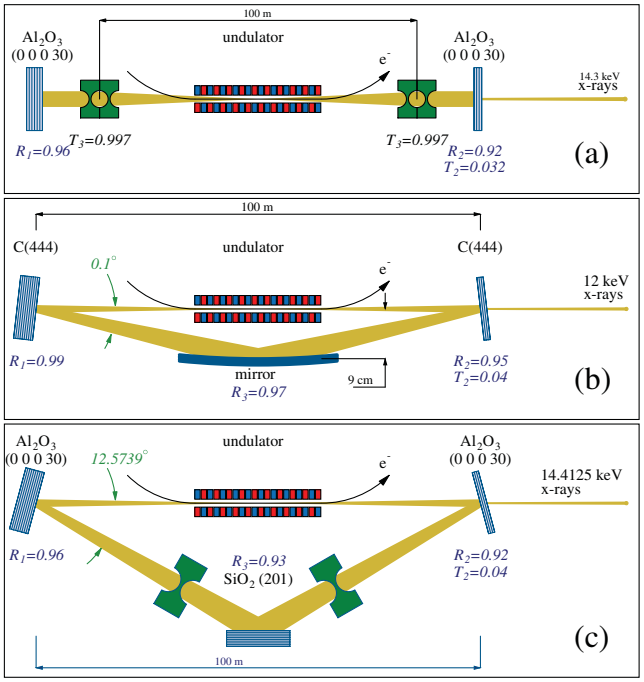

FIG. 2 (color). Schemes of x-ray cavities.

elements, the round-trip peak reflectivities are 87%, 91%, and 81% for schemes (a),(b), and (c), respectively. With these reflectivities the XFEL-O can operate if $g \gtrsim 30\%$. In all these cases, the out-coupling fraction is about 4%.

Out of several possible operating modes of an ERL [4], the *high coherence* mode is best suited for an X-FELO. The bunch parameters in this mode are: charge $Q = 19$ pC, normalized transverse emittance $\varepsilon_{nx} = 0.82 \times 10^{-7}$ m, rms energy spread $\sigma_{\Delta E} = 1.4$ MeV, and rms length $\tau_{el} = 2$ ps. These beam parameters are assumed to be the same for the 7-GeV APS ERL [6], since they are invariant under acceleration. The value of ε_{nx} is smaller by about 1 order of magnitude than that achieved for high-gain FELs [16]. However, we can be optimistic about achieving a smaller emittance since the peak current in our case is smaller by almost 3 orders of magnitude. An optimization study of a laser-driven, high-voltage dc gun shows that the bunch parameters listed above are feasible for 19 pC $\leq Q \leq$ 60 pC [17].

The X-FELO performance was studied by analytical calculation and by simulation using the GENESIS code [18]. We assume that the FEL mode in the cavity is Gaussian with the waist at the center of the undulator. For the electron beam, we assume that focusing is absent, the distribution is Gaussian, and the envelope parameter at the waist β^* is the same as the Rayleigh length Z_R of the FEL mode. The gain formula in Ref. [19] can then be greatly simplified. The intracavity power at saturation P_{sat} is determined by GENESIS simulation to be the power at which $(1 + g)r = 1$.

Table I gives some X-FELO examples. The beam parameters ε_{nx}, $\sigma_{\Delta E}$, and τ_{el} are assumed to be those listed above. The undulator parameters are: K-deflection parameter, λ_U-undulator period, N_U-number of periods, and $L_U = N_U\lambda_U$-undulator length. The wavelength for the fundamental FEL harmonic is $\lambda_1 = (1 + K^2/2)\lambda_U/2\gamma^2$ where γ is the electron energy E divided by the electron's rest energy. The undulators in the table can all be constructed using steel poles and Ne-Fe-B magnets with a gap of 5 mm [20]. The values of $Z_R = \beta^*$ given in the table are that corresponding to the maximum gain; it is about 10 m for the cases studied here. The low-power gain computed analytically, g_{th}, and by simulation, g_{sim}, agree reasonably well. The last two rows of the table show that the gain is higher at higher energy since both the geometrical emittance and the relative energy spread become smaller. As shown later in the discussion of the temporal mode structure, the rms length of the x-ray pulse is about 0.85 ps. Assuming 4% output coupling, each output pulse then contains 0.9×10^9 photons.

We have assumed a straight undulator in the above. Higher gain may be possible with an optical klystron configuration [21]. Also, the polarization of the X-FELO can be modulated arbitrarily by employing a crossed undulator configuration proposed in [22] and demonstrated recently [23]. X-FELOs can also be designed at lower energies down to about 5 keV.

TABLE I. Performance of X-FELO. See text for explanation of symbols.

λ_1 (Å)	E (GeV)	Q (pC)	K	λ_U (cm)	N_U	Z_R (m)	$g_{\rm th}$ (%)	$g_{\rm sim}$ (%)	r (%)	$P_{\rm sat}$ (MW)
1	7	19	1.414	1.88	3000	10	26	28	90	19
1	7	40	1.414	1.88	3000	12	55	66	83	21
0.84	7.55	19	1.414	1.88	3000	12	26	28	90	20
0.84	10	19	2	2.2	2800	10	42	45	83	18

To study the mode evolution of the X-FELO, GENESIS code was modified to add propagation in free space between the undulator and the mirrors, frequency filtering and reflection by mirrors, and focusing. To reduce the CPU time, a short time window of 25 fs was chosen. The resulting frequency interval is larger than the bandwidth of the crystals, and thus only one frequency component is present after reflection. Therefore, the wave front is the same over the entire time window, and only one single wave front needs to be propagated. Even with this simplification, simulation of a single pass took about two hours with a 25-node computer cluster at UCLA. A full tracking from initial spontaneous emission to final saturation took about one month. Figure 3 shows the power as a function of the pass number. One sees that an exponential growth emerges from the initial randomness after about 100 passes.

The temporal structure of the mode can be studied by adapting the supermode analysis [24,25] to the case of a narrow cavity bandwidth, describing the spectral narrowing during the exponential growth. Let $\tau_{\rm el}$ and $\tau_{\rm opt}$ be the rms lengths of the electron bunch and optical mode, respectively. We also introduce the length $\tau_M = (\omega/\sigma_\omega^M) \times (\lambda/4\pi c) = 1/2\sigma_\omega^M$ corresponding to the rms frequency bandwidth of the optical cavity σ_ω^M. We neglect the slippage effect since the total slippage length $\tau_s = N_U\lambda/c$ is about 1 fs which is smaller than all other length scales. Suppressing the transverse dependence, the electric field amplitude at the end of the undulator at the $n^{\rm th}$ pass can be written as $a(n,\zeta)\exp(i\omega\zeta)$, where $\zeta = t - z/c$ is the time coordinate relative to the bunch center and $a(n,\zeta)$ is the slowly varying part of the amplitude. Upon reflection by the crystals, the amplitude is filtered in frequency domain and becomes, assuming $\tau_{\rm opt} \gg \tau_M$, $a_M(n,\zeta) \approx a(n,\zeta) + \tau_M^2 a(n,\zeta)''$, where the prime denotes $d/d\zeta$. The pulse is then displaced in time by u with respect to a fresh electron beam, and amplified. For simplicity we neglect the imaginary part of gain and write the amplitude gain as $0.5gU(\zeta)$, where $U(\zeta) = 1 - \zeta^2/(2\tau_{\rm el}^2)$ is a factor representing the electron density fall-off assuming $\tau_{\rm el} \gg \tau_{\rm opt}$. Also taking into account the loss $\alpha = 1 - r$, the amplitude at the $(n+1)^{\rm th}$ pass is $a(n+1,\zeta) = (1 + (gU(\zeta) - \alpha)/2)a_M(n, \zeta + u)$. By expanding in u and retaining only the lowest terms,

$$\frac{\partial a_n(\zeta)}{\partial n} = \left(\frac{1}{2}(g-\alpha) + u\frac{\partial}{\partial\zeta} + \tau_M^2\frac{\partial^2}{\partial\zeta^2} - \frac{g}{4\tau_{\rm el}^2}\zeta^2\right)a_n(\zeta). \tag{1}$$

The solution of this equation is $a_n(\zeta) = \exp[n\Lambda_m - u\zeta/(2\tau_M^2) - g^{1/2}\zeta^2/(4\tau_M\tau_{\rm el})]H_m(g^{1/4}\zeta/\sqrt{2\tau_{\rm el}\tau_M})$, where $H_m(x)$ is the Hermite polynomial, and the growth rate per pass is

$$\Lambda_m = (g-\alpha)/2 - (u/2\tau_M)^2 - 0.5\sqrt{g}(2m+1)(\tau_M/\tau_{\rm el}). \tag{2}$$

The fundamental mode $m = 0$ has the largest growth rate with a Gaussian profile, with the rms length $\tau_{\rm opt} = \sqrt{2\tau_{\rm el}\tau_M}/g^{1/4}$, corresponding to the bandwidth $\sigma_\omega^{\rm opt} = 1/2\tau_{\rm opt} = g^{1/4}/\sqrt{8\tau_{\rm el}\tau_M}$.

From Fig. 1, the full spectral width of a single crystal is about 10 meV. Thus the rms width of two crystals forming the optical cavity can be estimated as $\hbar\sigma_\omega^M = 10/\sqrt{4\pi} = 2.8$ meV. Taking $g = 0.3$ and $\tau_{\rm el} = 2$ ps, we obtain $\tau_M = 0.1$ ps, $\tau_{\rm opt} = 0.85$ ps, and $\hbar\sigma_\omega^{\rm opt} = 2.3$ meV.

To limit the reduction in the effective gain by the second term in Eq. (2) to within 1%, we require $u < 0.2\tau_M$, which becomes $u < 20$ fs in the present case. The tolerance in the timing of the electron beam is therefore 20 fs, and the corresponding tolerance in the optical cavity length is 3 μm. The angular tolerance $\Delta\theta$ of the mirror may be determined by requiring that the change of the optical axis of the cavity be less than one tenth of the rms mode angle. We obtain $\Delta\theta \le 0.8(Z_R/L_{\rm opt})^2\sqrt{\lambda/2L_U}$, where $L_{\rm opt}$ is the length of the optical cavity. Taking $L_{\rm opt} \simeq 100$ m, we find $\Delta\theta \le 8$ nrad. These tolerances are tight but should be achievable.

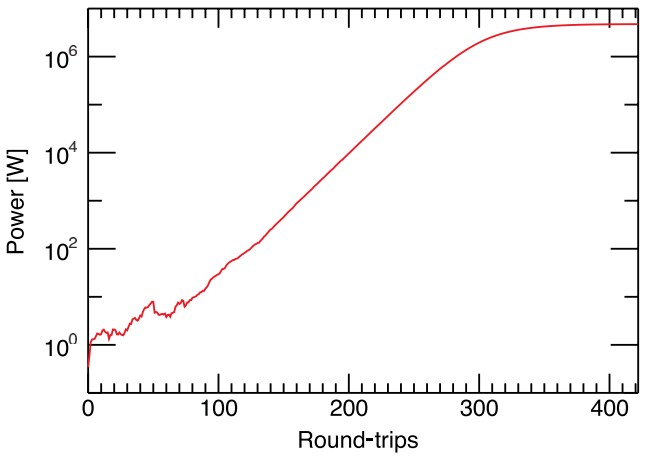

FIG. 3 (color). Evolution of intracavity peak power for the case corresponding to the first row in Table I.

The repetition rate f_{rep} of the X-FELO is 1.5 MHz when a single x-ray pulse stored in the optical cavity of a length $L_{\mathrm{opt}} \simeq 100$ m. There are several limitations in achieving a significantly higher rate. The first is due to the heat load on the crystals. The average power incident on the 70-μm rms radius hot spot receiving the coherent x rays is about 64 W. The power density at the hot spot is comparable to that of the undulators at the 3rd generation sources. Therefore, a repetition rate of $f_{\mathrm{rep}} \simeq 100$ MHz might be feasible. Another limitation arises due to the interference of the X-FELO on the ERL operation. The GENESIS calculation shows that the rms energy spread of the electron beam increases from 0.02% to 0.05% from the FEL interaction. Simulation predicts that the loss in the ERL return pass then becomes about 2×10^{-5} [26]. The ERL operation may become difficult with the increased energy spread and the enhanced loss level [27], but can be made feasible by stopping the deceleration for energy recovery at an energy higher than usual. Here we will assume that $f_{\mathrm{rep}} \simeq$ 100 MHz given by the heat load limit is feasible. With $f_{\mathrm{rep}} \simeq 1$ MHz, the X-FELO can only serve a single user station. With a higher f_{rep}, an X-FELO can provide beams to multiple user stations by various RF deflection techniques.

Compared to SASE from a high-gain FEL, the pulse intensity of an X-FELO is lower by two or 3 orders of magnitude, but its spectrum is narrower by more than 3 orders of magnitude. The pulse repetition rate is at least $\simeq$1 MHz, which is higher by at least 2 orders of magnitude than that of the high-gain, high-repetition-rate FEL using a superconducting linac [2]. The average spectral brightness of an X-FELO will be 10^{26} (10^{28}) photons/sec/(mm mr)$^2 \times$ (0.1% BW) assuming 1(100) MHz repetition rate. With these characteristics, X-FELOs for x rays in the range from 5 to 20 keV may open up new scientific opportunities in various research fiels, such as inelastic scattering [28] nuclear resonance scattering [15], x-ray imaging, and bulk-sensitive hard x-ray photoemission spectroscopy [29]. In particular, time-resolved measurement of Fermi surfaces via angle-resolved photoemission spectroscopy could be possible [30].

We thank Yusong Wang for his help with the GENESIS simulation, Ali Khounsary for discussions on heat load, and Fulvio Parmigiani for enthusiastic discussions on X-FELO applications. The research at Argonne is supported by the U.S. Department of Energy, Office of Science, Office of Basic Energy Sciences, under Contract No. DE-AC02-06CH11357 .

Note added in proof—The x-ray cavity schemes discussed here do not allow practically interesting tuning ranges in x-ray energy. However, a scheme which is tunable in a much broader energy range has been found by employing four crystals [31].

[1] LCLS Conceptual Design Report No. SLAC-R-593, 2002.
[2] R. Brinkmann, *Proc. of FEL06*, 24 (2006); http://www.jacow.org.
[3] T. Tanaka, Y. Asano, H. Baba *et al.*, *Proc. of FEL05*, 75 (2005); http://www.jacow.org.
[4] D. H. Bilderback, C. Sinclair, and S. M. Gruner, Synch. Rad. News **19-6**, 30 (2006).
[5] T. Kasuga, Proc. of APAC07, 172 (2007); http://www.jacow.org.
[6] M. Borland, G. Decker, A. Nassiri, and M. White, Proc. of PAC07, 1121 (2007); http://www.jacow.org.
[7] R. Colella and A. Luccio, Opt. Commun. **50**, 41 (1984).
[8] B. Adams and G. Materlik, *Proc. of Free Electron Lasers 1996*, II-24 (North Holland, Amsterdam, 1997).
[9] Z. Huang and R. Ruth, Phys. Rev. Lett. **96**, 144801 (2006).
[10] E. L. Saldin, E. A. Schneidmiller, Yu. V. Shvyd'ko, and M. V. Yurkov, Nucl. Instrum. Methods Phys. Res., Sect. A **475**, 357 (2001).
[11] See, for example, C. Brau, *Free-Electron Lasers* (Academic, San Diego, 1990).
[12] Yu. Shvyd'ko, *X-Ray Optics—High-Energy-Resolution Applications* (Springer Verlag, Berlin, New York, 2004).
[13] Yu. V. Shvyd'ko, M. Lerche, H.-C. Wille, E. Gerdau, E. E. Alp, M. Lucht, H. D. Rüter, and R. Khachatryan, Phys. Rev. Lett. **90**, 013904 (2003).
[14] B. Lengeler, C. Schroer, J. Tümmler, B. Benner, M. Richwin, A. Snigirev, I. Snigireva, and M. Drakopoulos, J. Synchrotron Radiat. **6**, 1153 (1999).
[15] Nuclear Resonant Scattering of Synchrotron Radiation, edited by E. Gerdau and H. de Waard (Baltzer, 1999/2000), Vol. 123–125 special issues of the Hyperfine Interact.
[16] R. Akre *et al.*, Phys. Rev. ST Accel. Beams (to be published).
[17] I. V. Bazarov and C. K. Sinclair, Phys. Rev. ST Accel. Beams **8**, 034202 (2005).
[18] S. Reiche, Nucl. Instrum. Methods Phys. Res., Sect. A **429**, 243 (1999).
[19] K.-J. Kim, Nucl. Instrum. Methods Phys. Res., Sect. A **318**, 489 (1992).
[20] K. Halbach, J. Phys. (France) **44**, C1-211 (1983).
[21] N. A. Vinokurov, *Proc. 10th Int. Conf. on High Energy Particle Accel.* 2, 454 (1977).
[22] K.-J. Kim, Nucl. Instrum. Methods Phys. Res., Sect. A **219**, 425 (1984).
[23] Y. Wu, Phys. Rev. Lett. **96**, 224801 (2006).
[24] G. Dattoli, A. Marino, A. Renieri, and F. Romanelli, IEEE J. Quantum Electron. **17**, 1371 (1981).
[25] P. Elleaume, IEEE J. Quantum Electron. **21**, 1012 (1985).
[26] M. Borland (private communications).
[27] L. Merminga, D. R. Douglas, and G. Krafft, Annu. Rev. Nucl. Part. Sci. **53**, 387 (2003).
[28] E. Burkel, Rep. Prog. Phys. **63**, 171 (2000).
[29] G. Paolicelli *et al.*, J. Electron Spectrosc. Relat. Phenom. **144-147**, 963 (2005).
[30] F. Parmigiani (private communications).
[31] K.-J. Kim and Y. Shvyd'ko, ANL Report No. AAI-PUB-2008-004.